

Partial persistence of memory in bubble breakup: incomplete universality acquired by broken symmetry

Ikumi Yoshino and Ko Okumura

Physics Department and Soft Matter Center, Ochanomizu University, 2-1-1 Ohtsuka, Bunkyo-ku, Tokyo 112-8610, Japan

(Dated: October 7, 2025)

When a water drop falls from a faucet, the drop is created with the formation of an axisymmetric constriction region, which thins down to breakup. Such formation of a fluid drop has been extensively studied as a representative of the singular dynamics widely observed in nature. The singular dynamics is often self-similar, i.e., shapes at different times collapsing onto a master curve after rescaling, and the self-similar dynamics has been categorized as either *universal* or *non-universal*: the master curve is *independent of or dependent on* the length scales that set the initial boundary conditions, as if memory is *erased or retained*. Here, we focus on the post-breakup dynamics and confine the system to break the axisymmetry, introducing three length scales, which leads to a third category of incomplete universality, where memory is partially retained: the master curve could be dependent on the smallest scale but independent of the other two scales. Affecting of only the smallest length scale on the master curve underscores the importance of scale separation for the emergence of universality. The present study suggests a promising direction for the study on the singular dynamics by exploring the symmetry.

Singular dynamics observed widely in nature from the gravitational collapse of a star [1] to the formation of a drop in dripping faucets [2] have attracted scientist in many fields such as cosmology [3], hydrodynamics, physics and mathematics [4–6]. One important feature of the singular dynamics governed by partial differential equations (PDEs) is *self-similarity*, reported in various phenomena including fluid-jet formation [7, 8] and drop coalescence [9–11]. The self-similarity is expressed as $h(t, x) = h_0(t)\Gamma(x/x_0(t))$ for the solution $h(t, x)$ of a PDE: although the shape defined by the plot x vs $h(t, x)$ for a given t changes with t , the rescaled shape defined by the plot $X = x/x_0(t)$ vs $Y = h(t, x)/h_0(t)$ at different times collapse onto a master curve $Y = \Gamma(X)$.

The self-similar dynamics is said to be *universal* or *losing memory*, when the master curve $\Gamma(X)$ is independent of the length scales that set the initial boundary conditions (BCs). This scenario is expected from the viewpoint of separation of scales: if the physics at small scales in length and time becomes important near the singularity, the dynamics may become independent from larger scales setting the BCs, as if memory (of the initial condition) is lost. The opposite case, in which $\Gamma(X)$ is dependent on the length scales, is said to be *non-universal* or *retaining memory*. This scenario is expected when the governing equation cannot define internal length scales.

One example of the *universal self-similar dynamics losing memory* is the breakup of a drop surrounded by less viscous fluid, where capillarity, inertia, and viscosity all come into play [12]: While the rescaled shape at different times collapse onto a master curve, the master curve is found to be independent of the single length scale that sets the BCs, the radius of a tube to create the drop. However, the breakup of bubble surrounded by more viscous fluid was shown to be a *non-universal self-similar dynamics retaining memory*, where the dynamics governed by the Stokes equation describing the viscous-

capillary balance [13]: The master curve does depend on the tube radius, reflecting that the Stokes equation cannot define length scales. Recently, this non-universal self-similar dynamics is found to exhibit crossover to a new universal self-similar dynamics governed by a wetting rim dynamics based on another viscous-capillary balance [14].

Here, we focus on the post-breakup dynamics and report a novel scenario in the singular dynamics: *the incomplete universality where memory is partially retained*. The key is a confinement, which breaks the axisymmetry of the previous cases. As a result, three independent length scales are introduced for the BCs. This is in contrast with the previous axisymmetric cases, which allow only one length that sets the BCs, the tube radius. The existence of three scales leads to a novel self-similar dynamics, in which the master curve depends on the smallest length but not on the other scales: the universality is incomplete with memory partially retained. This is also expected from separation of scales if the length scale on which the collapse to a master curve is observed is comparable to the smallest length scale setting BCs but much smaller than the other scales.

We show an example of this new class of the singular dynamics by experiments with a high quality. The novel scenario of the incomplete universality on the memory in singular dynamics revealed in the present study opens a new avenue for understanding singular dynamics widely observed in nature and underscores the importance of exploration of the symmetry in singular dynamics.

Experimental— The setup and experimental procedure are shown in Fig. 1 (a). We regard the phenomenon as a confined bubble breakup because, after air breaks up, the lower part detaches from the disk and becomes a bubble. The cell width and height (typically 9 and 12 cm, respectively) are much larger than the other length scales: the depth (or thickness) of the cell D , the thickness D_0 and the radius R of the disk. Note that D does not repre-

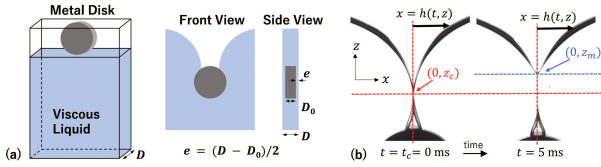


FIG. 1. (a) Experimental setup. A metal disk of thickness D_0 ($= 2.0 - 3.5$ mm) and radius R (10 to 15 mm) falls in the cell of thickness D (3 to 4.5 mm) filled with a viscous liquid of kinematic viscosity ν (1 to 50 St). The disk entrains air into the liquid, which finally detaches from the disk. The difference between D and D_0 defines the liquid film thickness e , indicated in the side view from the right edge of the front view. (b) Snapshots at breakup and after breakup illustrating the setting of axes for $(e, D_0, R, \nu) = (0.5, 3, 10, 1)$ in mm or St. $z = z_c$ is set to the origin of the z coordinate.

sent a diameter (but the cell depth), and D_0 is comparable to and a bit smaller than D with $e = (D - D_0)/2 < D_0$. We use polydimethylsiloxane (PDMS) for viscous liquid of kinematic viscosity $\nu = \eta/\rho$. The density ρ and the surface tension γ are slightly depending on viscosity η ($\rho \simeq 0.97$ g/cm³ and $\gamma \simeq 20$ mN/m). The density ρ_s of the metal disk is either is 7.7 g/cm³ (stainless: SUS430) or 8.7 g/cm³ (brass) with the density difference $\Delta\rho = \rho_s - \rho$. The cell is fabricated with acrylic plates of thickness 5 mm, using acrylic spacers whose thickness defines D . To capture the dynamics, we analyzed the images with Image J and self-made Python codes, which were obtained with a high-speed camera (FASTCAM Mini UX 100, Photron) with a lens (Micro NIKKOR 60 mm f2.8G ED, Nikon) at 1000 to 2000 frames per second (fps). The spacial resolution of the image is typically 50 pixels per mm or more.

We here summarize important points to realize high reproducibility. We need to achieve (1) the thickness e of the lubrication films on both surfaces of the disk to be equal, i.e., $e = (D - D_0)/2$, as indicated in Fig. 1 (a), (2) the initial velocity of the metal disk to be zero at the entry (initial velocity affects the results, especially for the pre-breakup dynamics), and (3) the contact angle of the surface of the disk to be zero (the contact angle affects the results). Accordingly, (1) we set a gate with the gap D_0 at the top of cell by placing two small plates of thickness e on the inside surfaces of the cell, (2) we fall the disk so that the bottom of the disk is initially in contact with the air-liquid interface, and (3) we wipe the oil on the surface of the disk after dipping to coat the surface by a thin layer of the oil.

Temporal change of the dynamics— In Fig. 2, we show typical snapshots before and after breakup in the present parameter range. A thin air film is formed slightly before breakup, as confirmed by the side-view snapshots obtained for a similar parameter set in our previous study on the pre-breakup dynamics [15]. In the post breakup of the present focus, the tip is sharp when seen from the front as in the snapshots at short times (just after the breakup), but becomes rounded with time, while our fo-

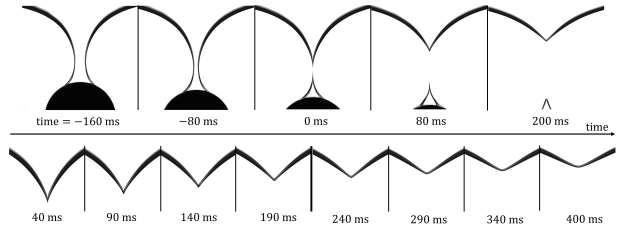


FIG. 2. Snapshots of entrainment of air by a disk into liquid, leading to breakup of a sheet of air for $(R, D_0, e, \nu) = (10, 3, 0.5, 10)$ in mm or St. In the top panel, overall time development is shown. In the bottom magnified snapshots, the sharp tip at short times become rounded with time, with the thick vertical line in the middle indicates the border. The time label 0 ms corresponds to $t = t_c$ defined in the text.

cus below is mainly on the regime after the breakup but before the tip becomes clearly rounded.

Shape of the air-liquid interface $h(z, t)$ — Figure 1 (b) explains the definition of the shape and the setting of space-time coordinate. The shape of air-liquid interfaces formed by air entrained by the disk are seen as the dark line with a finite thickness. In the present study, the inner edge of the right (or left) line is described by: $x = h(z, t)$ (or $-h(z, t)$). For further details, see Appendix A1.

The space-time coordinate is determined as follows (see Fig. 1 (b)). Before breakup the function $h(z, t)$ possesses a minimum with respect to z , which we call "the constriction point," at which $(x, z) = (h_m(t), z_m(t))$, i.e., $h_m(t) = h(z_m(t), t)$. At $t = t_c$, topology changes: The fluid breaks into two chunks at the constriction point $(h_m(t_c), z_m(t_c)) = (0, z_c)$, where $z = z_c$ will be set to the origin of the z coordinate. After $t = t_c$, the constriction point thus disappears and the dynamics of the interface of our focus is characterized by the tip point $(0, z_m - z_c) = (0, z_m)$. Experimentally, our time label 0 ms could deviate from the true $t = t_c$ at most 1 ms, which is set by frames per second in capturing images. See further details for Appendix A2.

The way of selecting the edge and the determination of time label 0 ms, detailed in Appendix A1 and A2, are technically important for data collapse presented below. Slight changes could deteriorate the quality of the collapse.

Dynamics of characteristic length scale— In Fig. 3 (a), we present the relation between z_m and t for various conditions, in which we can confirm an excellent reproducibility of the present measurement. For example, if we closely examine the data shown by blue diamond, we see several overlapping data points, which are generally obtained on different days.

In Fig. 3 (b), in which we show error bars for a set of data, we can confirm all the data in (a), which include the data for different e , D_0 , R , η , and $\Delta\rho$, can be well described by the following relation between dimensionless quantities:

$$z_m(t)/D = f(\Delta\rho g R t' / \eta) \equiv f(t' / \tau) \quad (1)$$

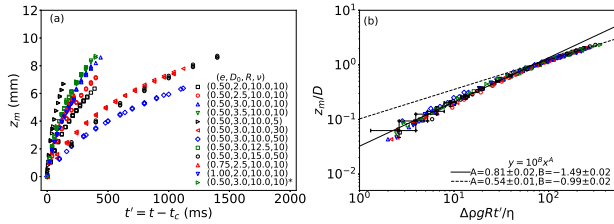


FIG. 3. (a) z_m vs. $t' = t - t_c$, where t_c is the critical time defined in the text for various parameters (e, D_0, R, ν) in mm or St. The data marked with a star (*) in the legend are those obtained for a different $\Delta\rho$ by using a brass disk instead of a disk of stainless steel. (b) Distinct data collapse by Eq. (1). All the data in (a) are plotted on rescaled axes, based on Eq. (1), demonstrating a clear data collapse with a quasi scaling-crossover between the regimes reasonably well characterized by the exponent $\Delta' \simeq 0.8$ and $1/2$, as indicated by the results of fitting where $y = z_m(t)/D$ and $x = \Delta\rho g R t' / \eta$.

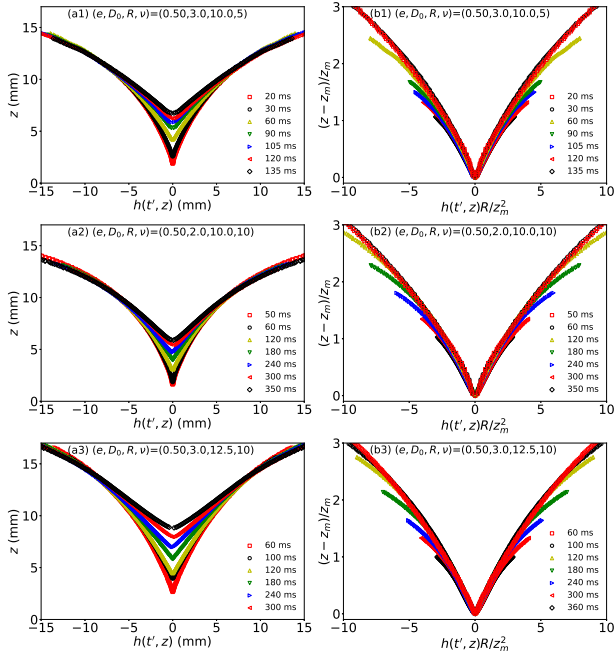


FIG. 4. (a1) to (a3) Temporal change of the interface $h(z, t)$ at $e = 0.5$ mm for the parameter sets $(D_0, R, \nu) = (3, 10.0, 5)$, $(1.0, 10.0, 10)$ and $(2.0, 12.5, 10)$ in mm or St. (b1) to (b3) The space-time dependent collapse of the shape by Eq. (2). The collapse near the tip persists for long time, while that away from the tip is observed only for short time.

with $\tau = \eta / \Delta\rho g R$, where a time label t' (which is positive at times after $t = t_c$) is defined as $t' = t - t_c$ (The dependence on $\Delta\rho$ is more explicitly shown in Fig. 6 (b3) below). We can further confirm in Fig. 3 (b) that the slope Δ' of the z_m - t' relation on log-log scales seem to exhibit a crossover from Regime I to Regime II: $\tilde{z}_m = \tilde{t}^{\Delta'}$ with $\tilde{z}_m = z_m/D$ and $\tilde{t} \simeq t'/\tau$, where $\Delta' \simeq 0.8$ in Regime I and $\Delta' \simeq 1/2$ in Regime II (results of fitting are shown in the plot), although the range of regimes are limited (especially in Regime II).

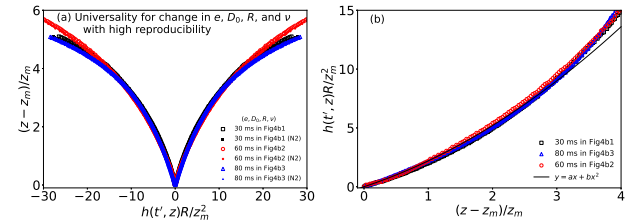


FIG. 5. (a) The master curves universal (and highly reproducible) for change in D_0 , R , and $\nu = \eta/\rho$ at $e = 0.5$ mm (but non-universal for change in e and $\Delta\rho$, as shown below in Fig. 6 (a3)). Shapes at earlier times in Fig. 4 are compared. The data marked as (N2) are basically obtained on a different day. (b) Right branches in (a) are shown with the axes interchanged, together with the results of fitting, where $y = h(z, t)R/z_m^2$ and $x = (z - z_m)/z_m$.

Self-similarity in the interface shape dynamics— In Fig. 4 (a1) to (a3), we show temporal changes of the interfacial shape after breakup for $e = 0.5$ mm but with different η , D_0 , and R . As seen in Fig. 4 (b1) to (b3), interface shapes after rescaling both axes by $h(z, t)R/z_m^2$ and $(z - z_m)/z_m$ are clearly collapsed onto a master curve, especially near the tip where $(z - z_m)/z_m \lesssim 1$. The collapse shown in (b) implies the following scaling form:

$$h(z, t) = \frac{z_m^2}{R} \Gamma \left(\frac{z - z_m}{z_m} \right) \quad (2)$$

As shown in Fig. 5 (a), the master curve near $t = t_c$ collapses well (and thus is reproducible) beyond the linear region near the tip up roughly to $(z - z_m)/z_m = 3$ even if parameters D_0 , R , and η are changed in a limited range with e fixed to 0.5 mm. The universal master curve seems to be linear near the tip but quadratic away from the tip. In fact, we can show the master curve is well described by $\Gamma(x) = ax + bx^2$ with $a = 1.8 \pm 0.2$ and $b = 0.4 \pm 0.05$ as shown in Fig. 5 (b) by a two-step fitting: We first determine a by fitting to the linear region near the tip (on log-log scales) and then determine b by fitting to the quadratic region after subtracting the linear component. Note that the confirmation of the collapse by Eq. (2) becomes very difficult for the shape very close to $t = t_c$, such as those at t with $t - t_c \lesssim 10$ ms, which is the order of the time resolution of our experiment limited by frames per second in capturing images. This is because z_m becomes very small and approaches the spatial resolution of our experiment, meaning that the error in estimating z_m becomes too large.

The collapse observed for the post-breakup dynamics ($t > t_c$) in Fig. 4 is regarded as space-time dependent if we notice that, by the present rescaling $h(z, t)R/z_m^2$ and $(z - z_m)/z_m$, shapes at times closer to $t = t_c$ are more strongly magnified, since z_m becomes smaller as $t \rightarrow t_c$. (1) Near the tip ($z = z_m$), the master curve is linear and the shape collapse to it persists for times rather away from the breakup ($t = t_c$). (2) Away from the tip ($z > z_m$), it is parabolic, but the collapse is limited

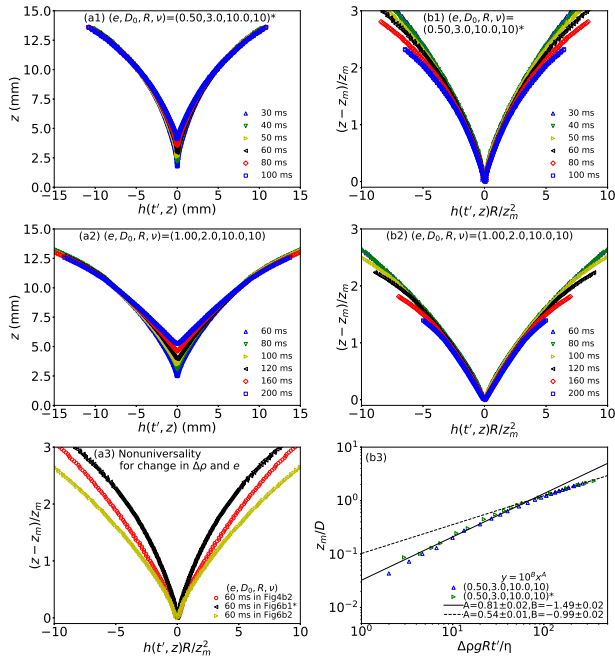


FIG. 6. (a1) and (a2) Temporal change of the interface $h(z, t)$ at $\Delta\rho$ and e different from those in Fig. 4 or Fig. 5: $(e, D_0, R, \nu) = (0.5, 3, 10, 10)$ in mm or St using a brass disk and $(1.0, 2.0, 10, 10)$ using a stainless disk. The star (*) in (a1) [as well as in (b1), (a3) and (b3) below] indicates the data obtained for different $\Delta\rho$ as in Fig. 3. (b1) to (b2) The space-time dependent collapse of the shape by Eq. (2). (a3) The master curves non-universal for change in e and $\Delta\rho$. Shapes in (b1) and (b2) are compared with a shape in Fig. 4 (b2) at an earlier time. (b3) z_m vs. $t' = t - t_c$. We extract from Fig. 3 (b) the data obtained for two different $\Delta\rho$'s (using the stainless and brass disks) at $(e, D_0, R, \nu) = (0.5, 3, 10, 10)$ in mm or St with the fitting lines in Fig. 3 (b), to clearly show the $\Delta\rho$ dependence. The results of the fitting are also shown with $y = z_m(t)/D$ and $x = \Delta\rho g R t' / \eta$.

only near the breakup time ($t \simeq t_c$). The space-time dependence is summarized as

$$\Gamma(X) \simeq \begin{cases} X & (X < 1) \quad \text{for long time after } t = t_c \\ X^2 & (X > 1) \quad \text{only for short time after } t_c \end{cases} \quad (3)$$

In other words, in Figs. 4 (and 6 below), the master curve is confirmed in the spacial region where the rescaled curves at the earliest time and that at the second earliest collapse: The spacial region of the master curve confirmed in this way is up roughly to $(z - z_m)/z_m = 3$.

The space-time dependent behavior of the master curve in Eq. (3) is preserved even if we change e and $\Delta\rho$ in a certain range, as shown in Fig. 6 (a1) to (b2). However, the master curve defined by shapes at earlier times in the range up roughly to $(z - z_m)/z_m = 3$ clearly depends on e and $\Delta\rho$ as demonstrated in Fig. 6 (a3), where we compare the shape at one early time with those obtained for a different e and a different $\Delta\rho$. We have also confirmed that the master curve at $e = 0.75$ mm,

for example, collapses onto neither the master curve at $e = 0.5$ mm nor that at $e = 1.0$ mm for a fixed $\Delta\rho$.

The incomplete universality: partial persistence of memory— The independence of the master curve from the length scales D_0 and R shown in Fig. 5 (a) and dependence on e shown in Fig. 6 (a3) reveal a new category of the incomplete universality for the memory of singular dynamics discussed in Introduction. This is because these lengths are the scales that set the initial boundary conditions of the present problem. In the present case, the master curve loses the memory on the scales D_0 and R , but retains the memory of the smallest scale e , which is quite natural from the viewpoint of scale separation, with remaining dependence on the material parameter on $\Delta\rho$ (and independence from η).

As a matter of fact, Fig. 6 (a3) shows that the two curves obtained for different e 's but the same $\Delta\rho$ become indistinguishable near the tip (although they seem distinguishable from the other obtained for a different $\Delta\rho$). This observation is in accord with our result of the two-step fitting: $(a, b) = (0.9 \pm 0.1, 0.6 \pm 0.05)$ for Fig. 6 (b1) and $(1.9 \pm 0.2, 0.7 \pm 0.05)$ for Fig. 6 (b2): $a = 1.9$ is indistinguishable from $a = 1.8$ (although $a = 0.9$ is distinguishable). This observation that near the tip universality tends to recover is also expected from separation of scales: very close to the tip, the characteristic length for the collapse tends to become small and thus become well separated even from the smallest length scale e .

The pre- and post-breakup dynamics— In the case of the viscous-capillary breakup of a bubble under no geometrical constraint, where the axisymmetric liquid-air interface is described by $r = h(z, t)$ in the cylindrical coordinate (r, θ, z) , the self-similar structure in the pre- and post-breakup can be expressed in the same form (see, e.g., Sec. 3.5.1 of [6]): $h(z, t) = |\tilde{t}'| \Gamma(z/|\tilde{t}'|^2)$ with a dimensionless time $|\tilde{t}'| \sim |t - t_c|$. This is in contrast with the confined case. The scaling structure for the pre-breakup, reported as $h(z, t) = 2|\tilde{t}'| \Gamma(z/|\tilde{t}'|)$ in [15], is significantly different from that for the post-breakup, $h(z, t) \simeq |\tilde{t}'|^{2\Delta} \widehat{\Gamma}(z/|\tilde{t}'|^\Delta)$, as seen from Eq. (2). This difference in structure may be related to the elongation of the constriction region near breakup. Because of the elongation, the critical time leading to a good collapse in the post-breakup becomes different from that in the pre-breakup.

Physics at the level of dimensional analysis— We may regard the present problem as finding a solution for Navier-Stokes equation for a viscous liquid, neglecting the role of air, giving initial BCs. It would be easier to give the initial BCs at the time $t = t_c$ rather than the time of the entry of the disk because after $t = t_c$ we can forget about the disk motion by giving the velocity of the tip of air at $t = t_c$. This velocity is given as $v_G \sim \Delta\rho g D^2 / \eta$ by balancing gravitational and viscous energy (per time) for the disk, $\Delta\rho g R^2 D v_G \sim \eta (v_G/D)^2 R^2 D$ (for $D \simeq D_0$), in the previous study on the pre-breakup dynamics [15]. In addition, from Eqs. (2) and (1) with the dependence on e of the master curve, we expect the

BCs involves $\Delta\rho, \eta, g, R, e$, and D but not on γ . Thus, we expect $h = f(t', z, \Delta\rho, \eta, g, R, e, D)$. Here, we have 9 dimensional variables, of which only 6 are independent, since the dimension of the unit of all variables can be derived from the three fundamental units, kg, m, and s.

From the Buckingham π theorem (see, e.g., Appendix C of [6]), we expect a relation $\pi_0 = \Xi(\pi_1, \pi_2, \dots, \pi_5)$, where π_i 's are 6 independent dimensional variables and Ξ is a dimensionless function. We select these dimensionless variables as follows. A natural characteristic scale in the z direction is z_m , from which we define $\pi_1 = z/z_m - 1$. A natural unit h^* (in the x direction) for h can be introduced through a curvature relation, $1/R \sim h^*/z_m^2$, from which we set $\pi_0 = h/h^*$. To select the remaining 4 independent variables, we focus on 4 length scales: $l = \eta/(\Delta\rho g t')$, R , e , and D , which are normalized by z_m to determine 4 dimensionless variables, π_2, \dots, π_5 . In this way, to be consistent with our experiment, we may arrive at $h = \frac{z_m^2}{R} \Xi((z - z_m)/z_m, l/z_m, R/z_m, D/z_m, e/z_m)$. Here, we may expect that near the breakup point where $z_m \sim (t')^{\Delta'}$ with $0 < \Delta' < 1$ is small so that the right-hand side of the equation becomes independent of the second to the fourth dimensionless variables (with $l/z_m \rightarrow \infty$ and $R/z_m, D/z_m \rightarrow 0$ but with a finite e/z_m).

In this way, the dimensional analysis provides a natural understanding of the scaling structure in Eq. (2) with the function Γ dependent on e but not on R and D , based on which structure we proposed the novel scenario of the incomplete universality. Although the present analysis cannot determine the scaling exponents (such cases are known as the self-similarity of the second kind [5]), a renormalization group analysis recently developed for the non-confined bubble breakup [16] will be promising to determine the exponents and to elucidate the origin of the scaling crossover in the present study.

Importance of exploring symmetry— We stress here that it is becoming clear that the present experimental system that can break the axisymmetry contains extremely rich physics. In the previous studies [15, 17, 18], three distinct regimes have been found by changing the range of confining length scales: the sheet-forming regime with breakup, the corn-forming regime with and without breakup. In the first and second, a sheet and a corn of air (which are both non-axisymmetric) are respectively formed at the constriction point leading to breakup, while, in the third, a corn detaches from the disk without appearance of the constriction point. In the third, in particular, analogy with critical phenomena is deeply explored to find the exponents are dependent on a length scale, which is a novel feature not found in the first and second regimes. In all of the three studies [15, 17, 18], we focus on the pre-detachment dynamics where detachment includes breakup. In the present study, we focus on the post-breakup for the first time, while, experimentally, the post-breakup dynamics has not been explored even in the non-confined case. As a result, we found a self-similar structure significantly different from those in pre-breakup dynamics as seen above and successfully ob-

tained the data strongly supports the novel scenario of the incomplete universality.

The remarkable physical richness of the present experimental system was uncovered by breaking of symmetry, which reminds the importance of symmetry and dimensionality in critical phenomena [19, 20]: a myriad of universality classes have been found by exploring symmetry and dimensionality, which has propelled the developments of modern physics ranging from soft and hard condensed matter, non-equilibrium systems to active matter [21–24]. Given this, the present study suggests a promising direction for the study on the singular dynamics: *exploring the symmetry in confined geometries with drawing an analogy with critical phenomena*. This direction is all the more promising if we remind that the singular dynamics has been widely observed and confinement is involved in many cases of natural phenomena and industrial processes ranging from geology and petroleum industry to microfluidics with applications such as in medicine and biochemistry [25–28].

Acknowledgments— This work was supported by JSPS KAKENHI Grant Number JP19H01859 and JP24K00596.

APPENDIX

A1: Definitions of the shape function h — The inner edge by which we define the shape corresponds to the contact line on the front surface of the back cell wall, whose surface is totally wetting (thin layer of oil exists ahead of "the contact line"). The relation $x = h(z, t)$ represents the shape outlined by the contact line on the back cell plate.

We here explain why the inner edge of the dark line corresponds to the contact line. In fact, the shape of the liquid-air interface is three dimensional: it should be a function of y : $x = \tilde{h}(t, z; y)$ with $h(z, t) = \tilde{h}(t, z; y = D)$, where $y = 0$ and $y = D$ respectively correspond to the back surface of the front cell plate and the front surface of the back plate. This implies that the curvature $\partial^2 \tilde{h}(t, x, z; y)/\partial y^2$ is negative (the surface of right branch is convex seen from the right liquid side), which goes to zero towards the tip: the outer edge corresponds $x = \tilde{h}(t, z; D/2)$ where $y = D/2$ corresponds to the middle plane between the inner surfaces of cell plates. This is because of continuity of surface, which is horizontal at places far away from tip, where the surface should be concave seen from the upper air phase. In addition, the contact line at $y = D$ is further away from the viewpoint compared with the line at $y = 0$, when seen from the front.

A2: Setting of space-time coordinates— The critical time t_c used in the analysis was determined as follows. Towards breakup, the constriction region starts to form a thin thread (when seen from the front), which finally pinches off, by which moment, we define $t = t_c$. Precisely speaking, the pinch-off is judged not by the inner edge

but the outer edge as indicated in Fig. 1 (b) left (the inner edge breaks up before the outer edge), but the positions z_c and z_m are determined by the inner edge (In Fig.1 (b), these positions are actually slightly above the dashed horizontal lines by the amount of the thickness of the line representing the interface). In addition, we set the time label 0 ms as the snapshot just before the pinch

off, using snapshots obtained at 1000 frames per second, which means there could be a difference at most 1 ms between our time label 0 ms and the actual critical time $t = t_c$. Because of this possible error in determining the origin of time, we avoid using snapshots too close to $t = t_c$ and use only those at $t \gtrsim 10$ ms.

[1] Matthew W Choptuik. Universality and scaling in gravitational collapse of a massless scalar field. *Physical Review Letters*, 70(1):9, 1993.

[2] XD Shi, M.P. Brenner, and S.R. Nagel. A cascade of structure in a drop falling from a faucet. *Science*, 265(5169):219, 1994.

[3] Tatsuhiko Koike, Takashi Hara, and Satoshi Adachi. Critical behavior in gravitational collapse of radiation fluid: A renormalization group (linear perturbation) analysis. *Physical Review Letters*, 74(26):5170, 1995.

[4] G. I. Barenblatt. *Scaling, self-similarity, and intermediate asymptotics*. Consultants Bureau, New York, 1979.

[5] Grigory Isaakovich Barenblatt. *Scaling*, volume 34. Cambridge University Press, 2003.

[6] Jens Eggers and Marco Antonio Fontelos. *Singularities: formation, structure, and propagation*, volume 53. Cambridge University Press, 2015.

[7] Benjamin W Zeff, Benjamin Kleber, Jay Fineberg, and Daniel P Lathrop. Singularity dynamics in curvature collapse and jet eruption on a fluid surface. *Nature*, 403(6768):401–404, 2000.

[8] Itai Cohen and Sidney R. Nagel. Scaling at the selective withdrawal transition through a tube suspended above the fluid surface. *Phys. Rev. Lett.*, 88(7):074501, Feb 2002.

[9] Maria Yokota and Ko Okumura. Dimensional crossover in the coalescence dynamics of viscous drops confined in between two plates. *Proc. Nat. Acad. Sci. (U.S.A.)*, 108:6395–6398; In this issue, PNAS, 108 (2011) 6337., 2011.

[10] JF Hernández-Sánchez, LA Lubbers, Antonin Eddi, and JH Snoeijer. Symmetric and asymmetric coalescence of drops on a substrate. *Physical Review Letters*, 109(18):184502, 2012.

[11] Paul R Kaneelil, Amir A Pahlavan, Nan Xue, and Howard A Stone. Three-dimensional self-similarity of coalescing viscous drops in the thin-film regime. *Physical Review Letters*, 129(14):144501, 2022.

[12] Jens Eggers. Universal pinching of 3d axisymmetric free-surface flow. *Phys. Rev. Lett.*, 71(21):3458, 1993.

[13] Pankaj Doshi, Itai Cohen, Wendy W. Zhang, Michael Siegel, Peter Howell, Osman A. Basaran, and Sidney R. Nagel. Persistence of memory in drop breakup: The breakdown of universality. *Science*, 302(5648):1185–1188, 2003.

[14] Amir A Pahlavan, Howard A Stone, Gareth H McKinley, and Ruben Juanes. Restoring universality to the pinch-off of a bubble. *Proceedings of the National Academy of Sciences*, page 201819744, 2019.

[15] Hana Nakazato, Yuki Yamagishi, and Ko Okumura. Self-similar dynamics of air film entrained by a solid disk in confined space: A simple prototype of topological transitions. *Physical Review Fluids*, 3(5):054004, 2018.

[16] Ko Okumura. A renormalization group analysis of bubble breakup. *Sci. Rep.*, 15(34507), 2025.

[17] Hana Nakazato and Ko Okumura. Air entrained into viscous liquid by a disk: Confinement induced suppression of breakup. *Physical Review Research*, 4(1):013150, 2022.

[18] Shoko Ii and Ko Okumura. *under revision*.

[19] J. Cardy. *Scaling and Renormalization in Statistical Physics*. Cambridge Univ. Press, Cambridge, 1996.

[20] N. Goldenfeld. *Lectures on Phase Transitions and the Renormalization Group*. Addison-Wesley Pub., Reading, 1992.

[21] Pierre-Gilles De Gennes and Pierre-Gilles Gennes. *Scaling concepts in polymer physics*. Cornell university press, 1979.

[22] Roberto Livi and Paolo Politi. *Nonequilibrium statistical physics: a modern perspective*. Cambridge University Press, 2017.

[23] Alexander Altland and Ben D Simons. *Condensed matter field theory*. Cambridge university press, 2023.

[24] Julien Tailleur, Gerhard Gompper, M Cristina Marchetti, Julia M Yeomans, and Christophe Salomon. *Active Matter and Nonequilibrium Statistical Physics: Lecture Notes of the Les Houches Summer School: Volume 112, September 2018*, volume 112. Oxford University Press, 2022.

[25] Andrea Parmigiani, Salah Faroughi, C Huber, Olivier Bachmann, and Y Su. Bubble accumulation and its role in the evolution of magma reservoirs in the upper crust. *Nature*, 532(7600):492–495, 2016.

[26] H.A. Stone, A.D. Stroock, and A. Ajdari. Engineering flows in small devices. *Annu. Rev. Fluid Mech.*, 36(1):381–411, January 2004.

[27] Saeed Shad, Majid Salarieh, Brij Maini, and Ian D Gates. The velocity and shape of convected elongated liquid drops in narrow gaps. *J. Petroleum Sci. Eng.*, 72(1):67–77, 2010.

[28] Shelley Lynn Anna. Droplets and bubbles in microfluidic devices. *Annual Review of Fluid Mechanics*, 48:285–309, 2016.